Program Digest, 2019 IEEE International Ultrasonics Symposium (IUS)
Glasgow, Scotland, October 6-9, 2019

Multiparametric Ultrasound for the Targeting of Prostate Cancer using ARFI, SWEI, B-mode, and QUS

D. Cody Morris*, Derek Y. Chan*, Hong Chen†, Mark L. Palmeri*,
Thomas J. Polascik‡, Wen-Chi Foo∧, Jiaoti Huang∧, Jonathan Mamou†, Kathryn R. Nightingale*
*Department of Biomedical Engineering, Duke University, Durham, NC, USA,
† Lizzi Center for Biomedical Engineering, Riverside Research, New York, NY, USA
‡ Department of Surgery, Duke University Medical Center, Durham, NC, USA
∧ Department of Pathology, Duke University Medical Center, Durham, NC, USA
Email: cody.morris@duke.edu

***Abstract*—Prostate cancer diagnosis using standard transrectal ultrasound (TRUS) and systematic biopsy is challenging. To improve the performance of TRUS imaging, we combined it with acoustic radiation force impulse (ARFI) imaging and shear wave elasticity imaging (SWEI) to enhance lesion contrast into a multiparametric ultrasound (mpUS) synthesized image using a linear support vector machine (SVM). The SVM was trained on one subset of patients (N=15) and applied to a second subset (N=15) imaged with a different transducer. mpUS imaging identified 79% of clinically significant PCa in the second cohort with a PPV of 95%.**

I. Introduction & Background

Prostate cancer (PCa) is the second leading cause of cancer related death and the primary cause of new cancer diagnoses for males living in the United States with an estimated 31,620 deaths and 174,650 newly diagnosed cases in 2019 [1]. PCa is typically diagnosed after a suspicious digital rectal exam (DRE) or elevated prostate-specific antigen (PSA) test via the gold standard transrectal ultrasound (TRUS) guided biopsy. TRUS guided biopsy consists of 10-12 biopsy cores acquired systematically throughout the prostate determined by the prostate anatomy, without any targeting of apparent cancerous regions [2]. The lack of targeting involved in the systematic approach to TRUS biopsy along with the sensitivity and specificity issues related to TRUS imaging leads to only 18-36% of men suspected of having PCa being diagnosed after their first biopsy visit [3].

To combat the limitations of standard TRUS, additional 3-D imaging methods with increased PCa contrast can be used to enhance lesion detectability. Acoustic radiation force impulse (ARFI) imaging and shear wave elasticity imaging (SWEI) are both elasticity-based techniques for identifying PCa which rely on acoustic radiation force (ARF) as the mechanical excitation for elasticity imaging. ARFI is an actively researched topic in the prostate cancer diagnosis field with work demonstrating its ability to identify 71% of clinically significant lesions present with high specificity toward clinically significant disease [4]. A drawback of both ARFI and other strain elastography methods are that they only provide a relative measure of tissue stiffness. SWEI, however, provides a quantitative estimate of the tissue stiffness which may be relevant in the clinical staging of PCa [5]–[8].

In this work, we use a classifier to synthesize a multiparametric ultrasound (mpUS) image volume which combines information from ARFI, SWEI, and standard TRUS and assess the combination's ability to identify PCa in a population of 15 patients with biopsy-confirmed PCa.

II. Methods

A. Prostate Volume Acquisition

Ultrasonic data were acquired in 30 patients with biopsy-confirmed PCa immediately preceding radical prostatectomy using a modified Siemens SC2000 (Siemens Medical Solutions, Mountain View, CA) and an Acuson ER7B or custom designed Siemens 12L4 transrectal ultrasound probe. The scanner and side-fire endorectal probe were paired with a modified CIVCO Micro-Touch stabilizer and rotation stage (CIVCO Medical Solutions, Kalona, IA USA) to acquire sagittal images of the prostate with a 1-1.5 degree angular spacing. The rotation stage was equipped with a stepper motor and custom optical angular feedback to rotate to the desired angle and ensure accurate measurement of the angle as each image was acquired [4]. All data were acquired under an institutional review board-approved study after obtaining written informed consent.

The data acquisition process was initiated once each patient was in the operating room and under anesthesia. The patient was oriented in a supine position with the legs positioned in stirrups. The entire volume of the prostate was angularly swept twice, where the patient-right to left rotation corresponded to the ARFI and SWEI combined sequence, and the patient-left to right rotation corresponded to a high quality B-mode sequence. All data acquired are inherently co-registered as the probe was not repositioned once the data acquisition was underway and the general anesthesia limited patient movement. After each data volume was processed, the volumes were scan converted using 3-D Slicer into a 0.15 x 0.15 x 0.15 mm^3 voxel size [9].

978-1-7281-4595-2/19/$31.00 ©2019 IEEE

TABLE I
THE ARFI PUSH EXCITATION PARAMETERS FOR THE ER7B AND 12L4 TRANSDUCERS

Transducer	Transmit Foci (mm)	Frequency (MHz)	Number of Cycles	F-number	Number of patients
ER7B	30, 22.5, 15	4.6, 4.6, 5.4	300, 300, 300	2.0, 2.0, 2.35	15
12L4	30, 22.5, 15	4.6, 4.6, 4.6	300, 300, 300	2.0, 2.0, 2.0	15

TABLE II
THE ARFI/SWEI HYBRID TRACKING CONFIGURATION FOR THE ER7B AND 12L4 TRANSDUCERS

Transducer	Transmit Focus (mm)	Frequency (MHz)	F-number	PRF (kHz)	ARFI Track Spacing (mm)	SWEI Track Offset (mm)	SWEI Track Spacing (mm)	Track Duration (ms)
ER7B	60	5.0	3.0	8.0	0.17	1.89	0.76	5
12L4	60	5.0	2.0	10.0	0.17	2.01	0.78	4.3

B. ARFI and SWEI Processing

The ARFI and SWEI combined sequence was described by Palmeri et al. and the parameters for the ARFI push excitation are included in Table I [4]. To summarize, a three focal zone combined ARFI push excitation was used to create an elongated depth of field for ARFI displacement generation [10]. Four ARFI tracking beams were placed inside the beam width of the push excitation. Twelve SWEI tracking beams were split into two groups of six tracking beams which were positioned to the left and right of the ARFI push excitation. For each group of 6, the beams were laterally offset from the push and spaced approximately one beamwidth apart [6]. The tracking lines were repeated over 4-5 ms to acquire displacement data through time. The ARFI push excitation and the corresponding 16 tracking line ensemble was repeated 82 times across the transducer to create a 55 mm lateral field of view. The sequences used were slightly different based on whether the ER7B or the 12L4 was used, these differences are also noted in Tables I and II. Data acquired using these sequences were captured as in-phase and quadrature (IQ) data.

For both the ARFI and the SWEI data volumes, Loupas' phase shift estimator was used on the acquired IQ data to calculate the displacements progressively through time at each location [11]. To limit the impact of noise, a correlation coefficient threshold of 0.95 was applied to exclude spurious displacement estimates. The progressively tracked displacement data were integrated through time to calculate the displacement through time profile for each position. Depth dependent gain was also applied to the ARFI data to account for attenuation and focal effects [12]. The ARFI data were histogram equalized to enhance lesion contrast.

The SWEI data were processed using techniques described by Manduca et al. [13], Lipman et al. [14], Song et al. [15], and Chan et al. [16]. The progressively tracked displacement data were low pass filtered with a phase-preserving 2^{nd} order Butterworth filter using a cutoff frequency of 1.5 kHz and 3D directionally filtered to minimize the impact of reflected waves [14]. 2D vector tracking was used to estimate the shear wave speeds at each location [15]. Overlapping track locations from neighboring ARFI excitation ensembles were used to average the noise on individual shear wave speed estimates. Finally, speed estimates greater than 12 m/s or with correlation coefficients less than 0.6 were discarded.

C. B-mode acquisition

In the patient-left to right sweep, a high-quality B-mode acquisition was used. 126 transmits which spanned the 55 mm field of view were used with 7:1 parallel receive tracking and coherent beamforming. For both transducers, a 7.0 MHz transmit frequency was used with an F/3 focal configuration [4]. F/1 dynamic receive was used for the receive beamforming. The B-mode data was processed by applying median filters both axially and laterally and by rescaling the log compressed data at each voxel from 0 to 255.

D. Histology

Post imaging, all prostates were radically excised, whole mounted, and stained with hematoxylin and eosin (H&E) for histologic analysis. The prostates were sliced apex to base with each slide being spaced approximately every 3 mm. An Epson 750 Pro scanner (Epson America, Long Beach, CA, USA) was used to scan the histology slides individually. Trained pathologists identified the Gleason grade of PCa foci along with benign prostatic hyperplasia (BPH) and atrophy. An identified lesion was considered clinically significant if its Gleason grade was greater than or equal to 7 or was larger than 0.5 mL. The histology slides were not registered with the data volumes due to slice thickness and orientation variability. Instead, a 27-region model determined by the anatomy of the prostate was used to localize the center of each lesion in each prostate [17].

E. PCa Identification and Classifier Training

In each ER7B case, the index lesion and a healthy region were identified and conservatively segmented using 3D Slicer for ARFI, SWEI, and B-mode volumes based on cognitive fusion with histologically determined ground truth [9]. The intersection of the three segmentations was used to identify the subset of voxels with the highest confidence for their suspected class. Of these 15 cases, 4 patients did not have any identifiable healthy prostate tissue. Seven classifiers, listed in table III, were applied to the normalized intersection data. These classifiers were explored because of their simplicity,

TABLE III
CLASSIFIER PERFORMANCE

Classifier	Validation Accuracy (%)
Linear Discriminant Analysis	88.8
Linear SVM with SGD	**90.3**
Quadratic Discriminant Analysis	89.3
K-Nearest Neighbors (k=5)	89.5
Simple Decision Tree	87.9
Random Forest	89.0
Multilayer Perceptron (hidden layers of 10 and 5)	90.2

ease of implementation, and ease of interpretation. 11-fold cross validation was applied to the classifiers where in each fold, a patient's complete healthy and lesion data set was excluded from the training of the classifier and used to assess its performance. Validation accuracy was assessed as the validation data set was balanced between voxels labeled as lesion and healthy.

F. Image Combination and Testing

The highest performing classifier was chosen and used to weight and combine ARFI, SWEI, and B-mode data into an mpUS volume. The weighting was applied to the 15 12L4 cases which were not used in the training phase. For each patient, all three modalities were normalized in the same fashion as pre-training, and then combined based on the weights determined by the classifier. This mpUS data was examined in 3D Slicer and the centers of any apparent lesions were identified [9]. The location of each lesion was determined based on the 27-region model of the prostate [17]. The PCa locations in the mpUS data were compared to the locations from the histology analysis and considered to be a successful match if both the mpUS and histology were within nearest-neighbor regions [4].

III. RESULTS & DISCUSSION

Table III contains the validation accuracy of each classifier examined in this study. All accuracies are comparable between 87.9% and 90.3%, indicating that the choice of classifier would not greatly impact the resulting mpUS data. The stochastic gradient descent (SGD) linear support vector machine (SVM) was chosen for the remaining analysis on the 12L4 test data as it slightly out-performed the other classifiers and was relatively simple to implement and understand. This linear SVM resulted in the straightforward combination scheme of multiplying the normalized ARFI, SWEI, and B-mode data by -2.5, 3.1, and -1.4, respectively, and summing the volumes. As in the normalization process, the data was shifted to be 0 mean and unit standard deviation, the absolute value of these weights indicate the relative importance of the three original data volumes. By using the SVM to determine the weights used in summing the ARFI, SWEI, and B-mode images without applying a final threshold to identify a given voxel as cancer or healthy, we allow the inherent contrast in the three separate modalities to be assessed by the reader in the summation.

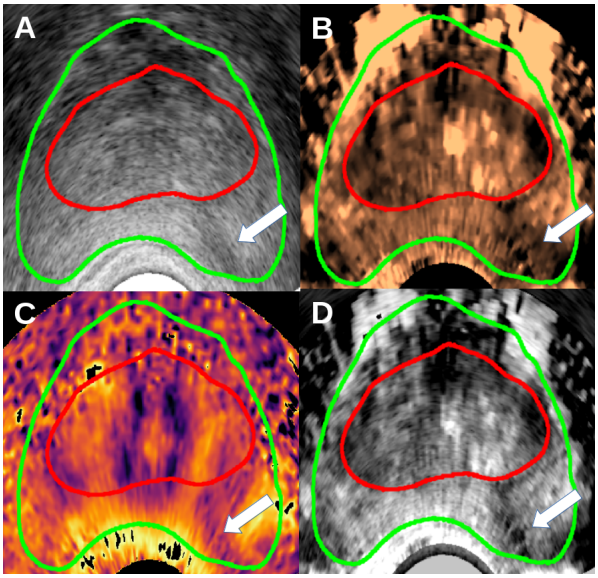

Fig. 1. Sample B-mode (A), ARFI (B), SWEI (C), and mpUS (D), registered images demonstrating structural concordance. The capsule (green) and central gland (red) are identified along with a suspicious region (white arrow).

Sample axial images of the B-mode, ARFI, SWEI, and mpUS volumes are shown in Figure 1. By not thresholding the data based on the SVM, we allow for aspects of texture, symmetry, and border delineation to be considered in the identification of PCa.

The analysis of the lesions identified with mpUS is included in Figure 2. A lesion was determined clinically significant if its Gleason grade was greater than or equal to 7 or was larger than 0.5 mL. In the 15 patients analyzed, 24 lesions were identified as clinically significant by histology, 19 of which were detected by mpUS. Although mpUS only identified 79% of the clinically significant cancer, of the 20 lesions identified by mpUS, only one was not clinically significant resulting in a positive predictive value(PPV) of 95%.

Characteristics of the missed mpUS lesions are identified in Figure 3. These lesions correspond generally to cases where the image quality pre-summation was lacking, the lesions were in the anterior of the prostate, or the lesions were a large portion of the entire prostate and standard practices failed to identify them. In the cases where the PCa is a substantial portion of the overall volume, examining the SWEI data volume and noting the underlying shear wave speeds, which have not been contrast enhanced, would help in identifying the suspicious regions.

IV. LIMITATIONS

The ground truth for PCa was identified in whole mount histology following radical prostatectomy and due to imperfect registration was limited to identifying the center of a lesion into one of 27 regions. This limits the patients recruited to the study to those with confirmed significant disease which may introduce a bias into the assessment of mpUS lesion detectability as every patient had at least one clinically sig-

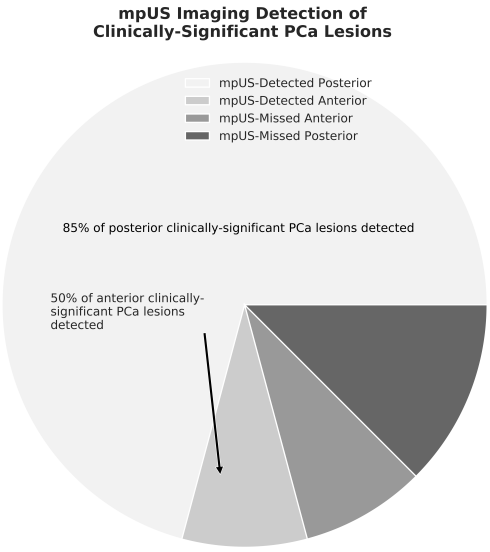

Fig. 2. Pathologists identified clinically significant lesions in the 15 12L4 patients. This included 4 identified as anterior lesions and 20 as posterior lesions. mpUS was able to detect 50% of the anterior lesions and 85% of the posterior lesions.

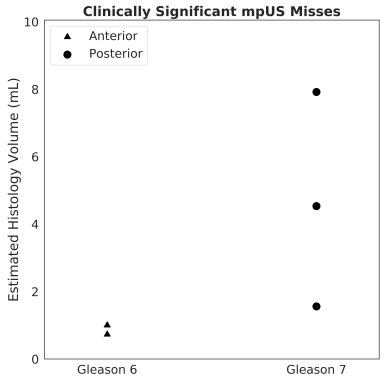

Fig. 3. Lesion volume versus Gleason grade for the clinically significant cancers that were not detected in the mpUS data.

nificant cancer. The poor registration of histology to the data volumes also limits the ability of more advanced machine learning techniques for identifying PCa as many of them require absolute truth or a large number of patients.

V. Conclusion

Creating a synthetic mpUS image volume using a linear SVM allowed for the native contrast of the input volumes to shine through to the combination. The specific combination of ARFI, SWEI, and TRUS was also transferable between two different transducers. mpUS imaging was able to identify 79% of clinically significant PCa in a subset of 15 patients with a PPV of 95%. Although mpUS was not sensitive to small anterior lesions and posterior lesions which were large enough to suppress the surrounding contrast, this study demonstrates the clinical value of mpUS as it has high specificity for clinically significant PCa. Ongoing work involves extending this process to include information from quantitative ultrasound (QUS) and developing an mpUS-based prostate biopsy targeting system for PCa screening.

Acknowledgements

This work was supported by National Institutes of Health (NIH) Grants R01 CA142824, R03 EB026233, and T32-EB001040 and Department of Defense (DoD) Grant USAM-RMC award number W81XWH-16-1-0653. The authors thank Siemens Medical Solutions USA, Ultrasound Division, for their in-kind technical support.

References

[1] R. L. Siegel, K. D. Miller, and A. Jemal, Cancer statistics, 2019, *CA. Cancer J. Clin.*, vol. 69, no. 1, pp. 734, 2019.
[2] N. Mottet *et al.*, EAU-ESTRO-SIOG Guidelines on Prostate Cancer. Part 1: Screening, Diagnosis, and Local Treatment with Curative Intent, *Eur. Urol.*, vol. 71, no. 4, pp. 618 629, 2017.
[3] A. Elabbady and M. Khedr., "Extended 12-core prostate biopsy increases both the detection of prostate cancer and the accuracy of gleason score," *Eur. Urol.*, vol. 49, pp. 49-53, 2006.
[4] M. L. Palmeri *et al.*, Identifying Clinically Significant Prostate Cancers using 3-D *In Vivo* Acoustic Radiation Force Impulse Imaging with Whole-Mount Histology Validation, *Ultrasound Med. Biol.*, vol. 42, no. 6, pp. 12511262, 2016.
[5] R. G. Barr, R. Memo, and C. R. Schaub, Shear wave ultrasound elastography of the prostate: Initial results, *Ultrasound Q.*, vol. 28, no. 1, pp. 1320, 2012.
[6] S. Rosenzweig *et al.*, Comparison of concurrently acquired in vivo 3D ARFI and SWEI images of the prostate, *IEEE Int. Ultrason. Symp. IUS*, pp. 97100, 2012.
[7] O. Rouvire *et al.*, Stiffness of benign and malignant prostate tissue measured by shearwave elastography: a preliminary study, *Eur. Radiol.*, vol. 27, no. 5, pp. 18581866, 2017.
[8] C. Wei, *et al.*, "Performance Characteristics of Transrectal Shear Wave Elastography Imaging in the Evaluation of Clinically Localized Prostate Cancer: A Prospective Study," *J. Urol.*, vol. 200, pp. 549-558, 2018.
[9] A. Fedorov *et al.*, 3D Slicer as an image computing platform for the Quantitative Imaging Network, *Magn. Reson. Imaging*, vol. 30, no. 9, pp. 13231341, 2012.
[10] S. Rosenzweig, M. Palmeri, K. Nightingale, Analysis of Rapid Multi-Focal-Zone ARFI Imaging, *IEEE Trans Ultrason Ferroelectr Freq Control*, vol. 62, no. 2, pp. 280289, 2015.
[11] T. Loupas, R. Peterson, R. Gill, Experimental evaluation of velocity and power estimation for ultrasound blood flow imaging, by means of a two-dimensional autocorrelation approach, *IEEE Trans Ultrason Ferroelectr Freq Control* vol. 42 pp. 689699, 1995.
[12] M. L. Palmeri *et al.*, B-mode and Acoustic Radiation Force Impulse (ARFI) Imaging of Prostate Zonal Anatomy: Comparison with 3T T2-Weighted MR Imaging, *Ultrason. Img.*, vol. 37, no. 1, pp. 22-41, 2015.
[13] A. Manduca *et al.*, "Spatiotemporal directional filtering for improved inversion of MR elastography images," *Med. Image Anal.*, vol. 7, no. 4, pp. 465-473, 2003.
[14] S. Lipman *et al.*, "Evaluating the Improvement in Shear Wave Speed Image Quality Using Multidimensional Directional Filters in the Presence of Reflection Artifacts," *IEEE Trans Ultrason Ferroelectr Freq Control*, vol. 63, No. 8, pp. 1049-1063, 2016.
[15] P. Song *et al.*, "Fast Shear Compounding using Robust 2-D Shear Wave Speed Calculation and Multi-Directional Filtering," *Ultrasound Med. Biol.*, vol. 40, no. 6, pp. 1343-1355, 2014.
[16] D. Chan, *et al.*, "Prostate Shear Wave Elastography: Multiresolution Reconstruction Dependence on Push Beam Spacing," *IEEE Int. Ultrason. Symp. IUS*, 2018.
[17] L. Dickinson, *et al.*, "Magnetic Resonance Imaging for the Detection, Localisation, and Characterisation of Prostate Cancer: Recommendations from a Europen Consensus Meeting," *Eur. Urol.*, vol. 59, pp. 477-494, 2011.